Repulsive Particle Interactions Enable Selective Information Processing at Cellular Interfaces

J. Elliott,[1,2] H. Shah,[1] R. Belousov,[1] G. Dey,[1] and A. Erzberger[1,2,*]
[1]Cell Biology and Biophysics Unit, European Molecular Biology Laboratory, Meyerhofstraße 1, 69117 Heidelberg, Germany
[2]Department of Physics and Astronomy, Heidelberg University, 69120 Heidelberg, Germany

(Received 18 June 2025; accepted 20 October 2025; published 21 November 2025)

Living systems relay information across membrane interfaces to coordinate compartment functions. We identify a physical mechanism for selective information transmission that arises from the sigmoidal response of surface-bound particle densities to spatial features in adjacent external structures through a nonuniform binding energy. This mechanism implements a form of spatial thresholding, enabling the binary classification of external cues. Expansion microscopy measurements of nuclear pore complex distributions in *S. arctica* show signatures of such physical thresholding.

DOI: 10.1103/ywr6-mzz5

Living systems process information to adapt and respond to their environment [1–5]. Theoretical principles underlying biological information processing have been identified in gene regulation [6,7], biochemical signaling [8–14], and cell-fate patterning [15–22]. Yet beyond molecular circuits, *physical* interactions, mechanical properties, and geometrical relations also impact how living materials process information [23–32]. Physical degrees of freedom influence how cells navigate complex environments [33–37], internalize pathogens [38–40], or coordinate subcellular processes [24,41,42]. For example, migrating cells respond to gradients in the elastic properties of structures in their environment (durotaxis [43,44]), or the density of binding sites for specific adhesion molecules (haptotaxis, [43,45–47]) using biophysical interactions between adhesion molecules, cell membrane, cytoskeleton, and external binding sites to read out information about external spatial heterogeneities. However, the principles underlying such physically mediated signal processing are not well understood [48,49]. In particular, how physical interactions shape the encoding and transmission of spatially resolved mechanical signals is unclear.

In this Letter, we focus on physical interactions of surface-embedded particles at the interfaces of biological, membrane-enclosed systems [Fig. 1(a)]. We investigate how the spatial distribution of such particles selectively encodes information stored in the features of surrounding external structures, e.g., the proximity of binding sites, which can subsequently change internal cellular states such as polarity [50]. We identify how nonlinear relations due to particle interactions control the flow of information across the interface, whereby the interface itself functions as an information-processing layer in a hierarchical architecture.

Specifically, we find that particle interactions of the simplest type—short-range repulsion—create sigmoidal mappings between an input potential field and output particle distribution, providing a physical mechanism for binary thresholding reminiscent of thresholding filters in computer vision [65]. By deriving explicit expressions for the *gain* and *threshold* parameters of the filter, we identify how the system's physical properties, i.e., the effective size of the surface-embedded particles and their typical concentrations, control the transfer of information. We identify an optimal information-processing regime and find that diverse interface-associated protein complexes and macromolecular structures in cells operate within this regime. In particular, we experimentally measure the predicted sigmoidal distribution of nuclear pore complexes in the envelope of *Sphaeroforma arctica* nuclei [66], which form in response to interactions with the surrounding cytoskeleton [67]. Our results indicate that physical thresholding could facilitate information transmission in the coordination of biological processes across cellular and subcellular interfaces.

Repulsive particle interactions binarize binding energy profiles—We consider diffusive particles on a membrane, which interact with the environment by attaching to and detaching from adjacent binding sites. The densities of particles ρ_i in the bound ($i = \mathrm{b}$) and unbound ($i = \mathrm{u}$) states, with state energies ϵ_i, evolve according to mass-conserving reaction-diffusion equations [68–70]

$$\partial_t \rho_i = \nabla \cdot [D_i \nabla \rho_i + \beta D_i \rho_i \nabla (E + \epsilon_i)] + \mathcal{R}_i \qquad (1)$$

*Contact author: erzberge@embl.de

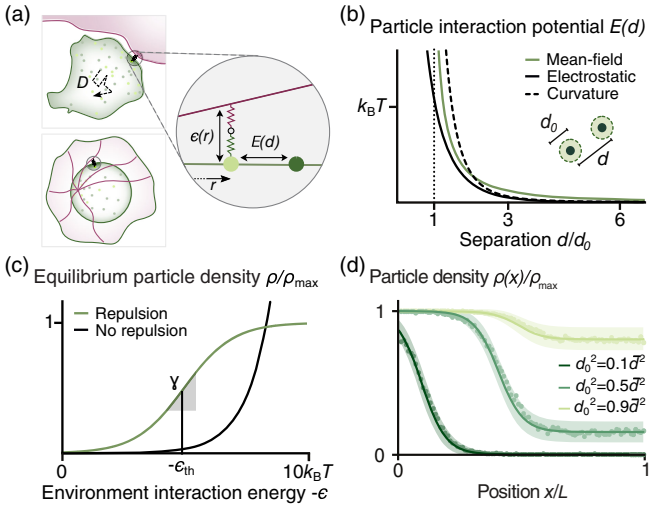

FIG. 1. The density of repulsive particles responds nonlinearly to changes in binding energy. (a) Particles on the surface of a membrane-enclosed compartment interact via a potential $E(d)$ that depends on their average separation distance d. Each particle can be either bound (light green circles) to an external structure (purple) or unbound (dark green circles), with binding rates set by a nonuniform interaction energy field ϵ. (b) The mean-field potential $E(d)$ captures short-range repulsion due to steric effects between particles of diameter d_0, similar to curvature-mediated interactions and shielded electrostatic repulsion ([51–58] and Supplemental Material [59], Sec. B b). (c) Repulsive particle interactions lead to a sigmoidal mapping between the particle-environment interaction energy ϵ and the particle density ρ, approaching the maximum density $\rho_{\max}$ in contrast to ideal, nonrepulsive particles. Vertical line and shaded triangle show the threshold ϵ_{th} and gain γ of the sigmoid. (d) For an interaction energy $\epsilon(x) = k_B T(20x/L - 10)$ on a domain of length L, this mapping produces sigmoidal equilibrium density fields [points from Metropolis-Hastings sampling (Supplemental Material [59], Sec. C 1 a), shading denotes two standard deviations].

driven by a mean-field interaction potential $E(\rho)$, which depends on the total density $\rho = \rho_b + \rho_u$, with the inverse thermal energy scale $\beta = (k_B T)^{-1}$ and, in general, density-dependent diffusion coefficients D_i [71]. The reaction terms describe transitions between the two states according to $\mathcal{R}_u = -\mathcal{R}_b = k_{\text{off}}\rho_b - k_{\text{on}}\rho_u$. To investigate how spatial heterogeneities in the environment influence the particle distribution, we consider nonuniform attachment rates $k_{\text{on}} = k_{\text{off}} e^{-\beta\epsilon}$, in which $\epsilon(\mathbf{r}) = \epsilon_b(\mathbf{r}) - \epsilon_u$ is a particle-environment binding energy field, with ϵ_u generally assumed spatially uniform.

From Eq. (1) and assuming no-flux boundary conditions, we obtain the *equilibrium* total density [[59,72] Sec. A]

$$\rho = \frac{1}{l^2} e^{-\beta E(\rho)} \left(1 + e^{-\beta\epsilon(\mathbf{r})}\right), \tag{2}$$

where the integration constant l is a length scale set by the conservation of the total particle number N over the whole membrane area A according to

$$N = \int_A \mathrm{d}A\rho. \tag{3}$$

This constraint determines the average separation distance between particles across the whole surface $\bar{d} = \sqrt{A/N}$. Equation (2) describes how the distribution of particles on the membrane surface responds to heterogeneities in mechanical and/or chemical properties of external structures, which give rise to a nonuniform $\epsilon(\mathbf{r})$. For example, an effective Hookean interaction energy could characterize the interactions of membrane-associated particles with external structures at a variable separation distance such that the nonuniform interaction energy captures spatial variations in binding site proximity.

Interparticle interactions influence how the density (2) responds to such external heterogeneities. Focusing on steric interactions (Supplemental Material [59], Sec. B a), we introduce an effective particle size d_0, imposing that each particle occupies an area d_0^2, and obtain the mean-field potential [Supplemental Material [59], Eq. (28)]

$$E(\rho) = -k_B T \ln(1 - d_0^2\rho) \tag{4}$$

which corresponds to the chemical potential difference between a volume-excluding lattice gas and the ideal gas [73,74]. By construction, the length scale d_0 determines the maximum possible density of the particles $\rho_{\max} = 1/d_0^2$. Although Eq. (4) assumes a volume-excluding lattice, the resulting potential also approximates well short-range repulsion arising, e.g., from curvature-mediated or shielded electrostatic interactions [Fig. 1(b)].

The equilibrium particle distribution resulting from Eqs. (2) and (4)

$$\rho(\mathbf{r}) = \frac{1 + e^{-\beta\epsilon(\mathbf{r})}}{l^2 + d_0^2(1 + e^{-\beta\epsilon(\mathbf{r})})}, \tag{5}$$

corresponds to a sigmoidal mapping between the binding energy field $\epsilon(\mathbf{r})$ and the density $\rho(\mathbf{r})$ [Fig. 1(c)]. In fact, we recover a Fermi-Dirac-like distribution, where the particle density at different positions is akin to the occupation number of energy levels, which are resolved along the surface according to $\epsilon(\mathbf{r})$: particles occupy the most energetically favorable spatial positions, given steric interactions and subject to mass conservation, leading to regions of high and low density. Therefore, the resulting particle distribution sigmoidally *filters* external heterogeneities, providing a physical mechanism for binarizing the binding-energy field. A cellular or subcellular interface could thereby read out spatial variations in, for example, the proximity of nearby structures.

The sigmoidal relation Eq. (5) is characterized by the gain, $\gamma := \max(\|\partial\rho/\partial\epsilon\|) = \beta l^2/[4d_0^2(d_0^2 + l^2)]$, and the threshold, $\epsilon_{\text{th}} := \operatorname{argmax}(\|\partial\rho/\partial\epsilon\|) = k_B T \ln[d_0^2/(d_0^2 + l^2)]$, [Fig. 1(c)], which depend on the two relevant length scales, the effective particle size d_0, and the average particle

separation $\bar{d}$, set by the total number of particles N. Note that through the integral over the entire membrane surface, constraint Eq. (3) incorporates a global dependence of the particle distribution on the interaction energy field into the normalization constant l, whose explicit expression follows $l \propto \sqrt{\bar{d}^2 - d_0^2}$ for uniform ϵ.

Particle size and total number tune information transmission—Could cells use Eq. (5) to sense the proximity of nearby structures? To investigate how the distance between a membrane patch and an adjacent set of binding sites can be conveyed by the particle density, we analyze the transmission of information in the presence of fluctuations.

In general, a noisy sigmoidal response can amplify an input signal close to the threshold, while rendering small energy variations unresolvable far from the threshold [Fig. 1(d)]. Repulsive particle interactions may thereby enable the *selective* transmission of information about interaction energies close to the threshold. When suitably optimized, such an information bottleneck can pick up specific task-relevant features of the input [75–78]. By controlling the gain and threshold, the biophysical parameters $\bar{d}$ and d_0 determine the amplified signal range, similar to the tunable resistors that shape the nonlinear mapping between input and output voltages in electronic audio processing [79].

To investigate how these parameters influence the compression of the original input, we first analyze the channel noise arising due to the microscopic particle dynamics. Discretizing space into boxes of area a indexed by $j = 1, 2, \ldots, B$ allows representing the particle and energy fields as random vectors which take realizations $\{\rho_j\}$ and $\{\epsilon_j\}$ from a finite set of density values and energy states [Fig. 2(a)]. Considering the limit of large particle numbers in a coarse-graining area element a, we approximate the conditional probability $P(\rho_j|\{\epsilon_k\})$ of a realization ρ_j given a set of binding energies by a Gaussian distribution with mean $\bar{\rho}_j(\{\epsilon_k\}) = \rho(\epsilon_j, l(\{\epsilon_k\}))$ given by Eq. (5), and standard deviation $\sigma_\rho(\bar{\rho}_j(\{\epsilon_k\})) = \sqrt{[1 - d_0^2\bar{\rho}_j(\{\epsilon_k\})]\bar{\rho}_j(\{\epsilon_k\})/a}$, such that the probability is conditioned on a realization of the entire binding energy vector through the parameter l ([80] and Supplemental Material [59], Sec. C 1). Metropolis-Hastings sampling of particle distributions numerically confirm these results ([81] and Supplemental Material [59], Fig. 1 and Sec. C 1 a).

To evaluate the level of selective signal amplification by the particle interactions, we compute the mutual information between the random vectors $\{\rho_j\}$ and $\{\epsilon_k\}$, given by

$$I = \sum_{\{\epsilon_k\}} \sum_{\{\rho_j\}} P(\{\rho_j\}, \{\epsilon_k\}) \ln \frac{P(\{\rho_j\}, \{\epsilon_k\})}{P(\{\rho_j\})P(\{\epsilon_k\})}, \quad (6)$$

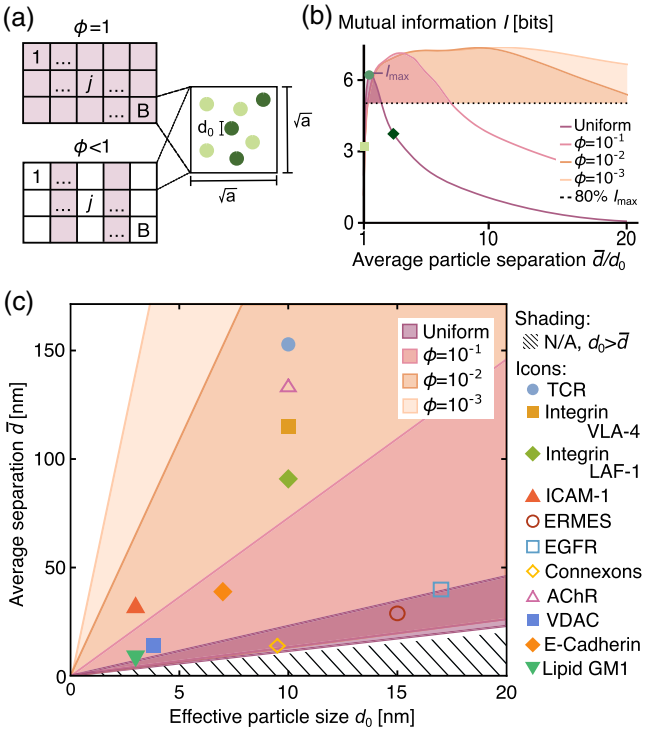

FIG. 2. Repulsive particle interactions threshold binding energy profiles. (a) We discretize the surface into B boxes of area a either with (purple shading) or without (no shading) binding sites, with ϕ the area fraction of the binding region. (b) The mutual information between the external field and the particle density profile shows a maximum as a function of $\bar{d}/d_0$, where the gain is high and the threshold energy is kept within the input range [computed for a system discretized into $B = 5$ boxes with $a = 10d_0^2$ as described in Supplemental Material Ref. [59], Sec. C 2]. The optimal information transmission regime—in which I is within 80% of its maximum—becomes larger as ϕ is decreased. Icons label parameter values used in Fig. 1(d). (c) The optimal information transmission regime is much larger for an actinlike area fraction $\phi = 10^{-2}$ [[59,82] Sec. D] (dark orange) than for uniform 2D sheets (dark purple). Macromolecular complexes in cells (colored icons, values from [[59,83–113] Table I]) indeed often associate with filamentous structures, such as the actin cytoskeleton (e.g., AChR, E-Cadherin).

in which the sums run over all possible realizations of the input and output sequences ([114], Chapter 2; Supplemental Material [59] Sec. C 2) The mutual information quantifies how well an output density field distinguishes different input fields. As such, rather than specifying one particular $\{\epsilon_k\}$, we must consider the probability distribution over *all* possible input fields, $P(\{\epsilon_k\})$, which takes a system-specific form depending on the statistics of binding energy variations across different environments. We consider in the following a uniform distribution over all realizations $\{\epsilon_k\}$ from a finite input range $\epsilon_{\min} < \epsilon_{\text{th}} < \epsilon_{\max}$, where the minimum binding energy $\epsilon_{\min}$ corresponds to the most favorable energy level, and the maximum binding energy $\epsilon_{\max}$ corresponds to the

least favorable input state, such that $P(\{\epsilon_k\}) = \prod_k P(\epsilon_k) = N_\epsilon^{-B}$, where N_ϵ is the number of discrete energy values from which the elements of $\{\epsilon_k\}$ are sampled. The joint probability $P(\{\rho_j\},\{\epsilon_k\})$ is the product of $P(\{\epsilon_k\})$ with the conditional probability $P(\{\rho_j\}|\{\epsilon_k\}) = \prod_j P(\rho_j|\{\epsilon_k\})$—where $P(\rho_j|\{\epsilon_k\})$ is approximated as discussed above. Numerical evaluation of Eq. (6) for a range of parameter values reveals an optimal regime of particle-mediated physical thresholding [Fig. 2(b), Supplemental Material [59] Sec. C 2]. Filters within this regime have gains large enough to overcome the channel noise and threshold energies within the input range.

In addition to the system parameters d_0 and $\bar{d}$, this optimal regime also depends on the spatial organization of interaction sites, which in biological systems are often irregular. While for uniform binding-site densities below the maximum particle density, the maximum transmitted information is reduced (Supplemental Material [59], Fig. 2), some nonuniform binding-site distributions can increase information transmission, and extend the optimal regime to a broader range of parameters. To identify, in particular, how information transmission is influenced when particles bind to structures such as cytoskeletal filaments, we consider binding sites confined to parallel lines that cover a fraction ϕ of the total membrane surface [Fig. 2(a), Supplemental Material [59] Sec. C 3] [115]. We find that lowering ϕ allows effective information transfer with fewer particles in the 2D membrane compared to the case of uniform binding sites [Fig. 2(b)], because—so long as the readout mechanism preserves the reduced dimensionality of the binding site geometry—the nonbinding region acts as a particle bath that buffers the particles used in the binding regions. As such, decreasing ϕ has a similar impact as decreasing $\bar{d}$, i.e., increasing the number of particles in the membrane [Fig. 2(b)]. In cellular contexts, protein *line* densities associated with such quasi-1D structures indeed influence many subcellular processes such as the generation of tension by motor proteins along filaments, or molecular events at cell-cell contact lines [116–120].

These optimal parameter regions for information transmission raise the question of where real surface-associated protein complexes and other macromolecular structures in biological cells fall. Bioimaging technologies are starting to overcome the challenges associated with visualizing nm-scale spatial arrangements of proteins along interfaces [121,122], and, in some cases, effective particle sizes and typical cellular concentrations have been reported or can be inferred from other measurements (Supplemental Material [59], Table I). Indeed, we find that proteins known to associate with actin fibers or bundles (AChR [123–125], E-Cadherin [126], TCR [127], ICAM-1 [128,129]) fall within the region in which information transmission from filamentous networks with an actinlike area fraction is optimal, whereas some proteins known to bind between neighboring cell membranes (connexons [130,131]) or subcellular membraneous structures (ERMES [99,132]) have sizes and surface densities that position them where information transmission is highest for uniform interaction sites [Fig. 2(c), dark orange and dark purple regions, respectively; Supplemental Material [59], Sec. D]. Precisely characterizing the information transmission capabilities of a particular system requires experimental measurements of the binding site geometry for a given readout mechanism.

Physical thresholding at the nuclear envelope—For large macromolecular structures, only a relatively small number of particles is required to form extended maximum-density regions. As a specific experimental example, we focus on nuclear pore complexes (NPCs) [133]. These protein complexes, approximately 100 nm in diameter, are embedded within the nuclear envelope—an intracellular membrane that forms the physical and regulatory interface between the cytoplasm and the nuclear interior [134,135]. In addition to controlling nucleocytoplasmic transport, NPCs interact with the extranuclear cytoskeleton to regulate intranuclear states, including gene expression [136–139]. Yet how the spatial distribution of NPCs influences information transfer between cellular and nuclear states remains unclear [140–145].

We measure how nuclear pore complex distributions respond to different configurations of the extranuclear microtubule cytoskeleton using expansion microscopy and immunostaining of *S. arctica* nuclei [Fig. 3(a), Supplemental Material [59], Fig. 3 and Sec. E, [146]] [67,147]. Quantifying the separation distance h between individual microtubule filaments and the nuclear surface reveals increasing height profiles from their anchor point at the pole towards the nucleus equator [Fig. 3(b)]. We estimate the NPC density profiles along the filament arc length by taking averages across clusters of similar filaments and fitting Eq. (5) to this data, assuming that the effective binding energy profiles arise from the combination of a fixed interaction energy, $\epsilon_{\mathrm{NPC}} = 25 k_{\mathrm{B}} T$, and an effective Hookean elastic contribution, such that the binding energy field is given by $\epsilon(s) = \epsilon_{\mathrm{NPC}} + \lambda_{\mathrm{NPC}}(h - h_0)^2/2$, with effective spring constant λ_{NPC} and resting spring length $h_0 = (84 \pm 15)$ nm (measured independently from electron microscopy images) [Fig. 3(c), Supplemental Material [59] Fig. 3] [148]. This assumption implies that heterogeneities in the interactions between NPCs and microtubules arise in this system primarily due to differences in the proximity of filaments to the nuclear envelope. We thereby obtain estimates for the effective NPC size $d_{0,\mathrm{NPC}} = (260 \pm 50)$ nm, and the spring constant characterizing the elastic interaction between NPCs and microtubule filaments $\lambda_{\mathrm{NPC}} = (0.04 \pm 0.03)$ pN nm^{-1} (Supplemental Material [59], Table III). Our estimates of the minimal NPC separation distance—which we further corroborated using focused ion beam-scanning electron microscopy imaging—are larger than their diameter, suggesting additional nonsteric repulsion effects, for example due to curvature-mediated interactions

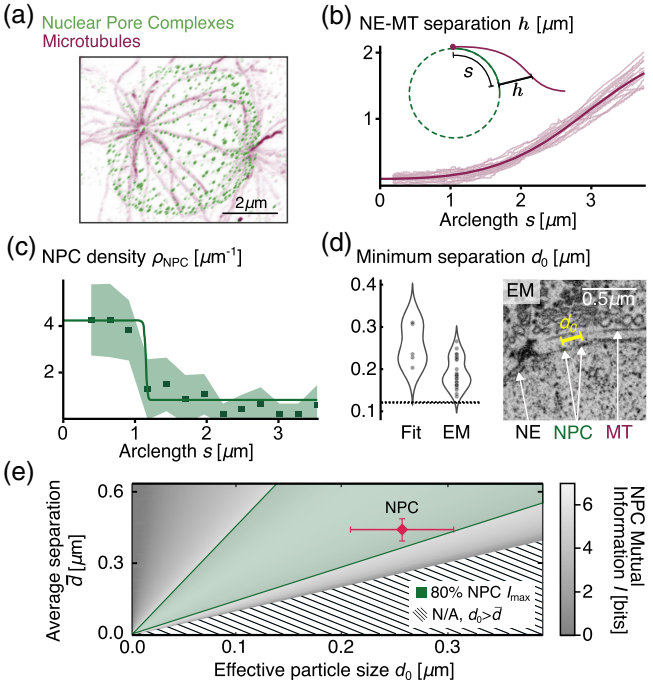

FIG. 3. Nuclear pore complexes (NPCs) form sigmoidal line densities along extranuclear microtubule filaments in *S. arctica* nuclei. (a) Ultrastructure expansion microscopy shows the spatial organization of immunofluorescently labeled microtubules (purple) and NPCs (green) on an *S. arctica* nucleus (maximum intensity projection) (Supplemental Material [59], Sec. E 1 b). (b) The shortest separation distance between the nuclear envelope (NE) and the microtubule (MT) filaments increases as a function of the arc length s away from the microtubule organizing center at the pole. Light purple: individual tracks for one of five clusters. Dark purple: rational-exponential reparameterization of these tracks (Supplemental Material [59], Sec. E 2 a). (c) Fitting (solid line) the measured NPC line density (dots) for the MT cluster in (b) with Eq. (5) yields parameter estimates for the effective spring constant λ and for the minimum NPC separation distance d_0 (Supplemental Material [59], Table III). Shaded area: 95% confidence interval. Other fitted profiles shown in Supplemental Material Ref. [59], Fig. 3. (d) Left: fit values for the minimum NPC separation d_0 compare well with independent measurements of d_0 from electron microscopy (EM) imaging, dashed line denotes the diameter of the complex 120 nm. Right: an example EM image with labeled features. (e) The fitted d_0 value, and the average NPC separation distance $\bar{d}$ measured from the data, indicate that NPC distributions can efficiently threshold microtubule proximity, given the measured filament density in this system $\phi = 0.21 \pm 0.03$.

arising from nuclear-envelope deformations close to the NPCs [Fig. 3(d)] ([67,149], Supplemental Material [59], Sec. E 2 and Table II).

Computing the transmitted information given a surface area fraction corresponding to that of the microtubule (MT) filaments at the nuclear envelope in this system ($\phi = 0.21$) reveals that their effective size and total number allow these NPCs to efficiently threshold the MT proximity profiles [Fig. 3(e); Supplemental Material [59], Sec. C 3].

Together, these results suggest that NPCs form sigmoidal density profiles along microtubule filaments due to their large effective size and fixed number [67,150–153]. We propose that the thresholded readout of filament proximity could coordinate intranuclear functions, consistent with observations that microtubule-nucleus interactions influence, e.g., chromatin organization, gene expression, and mitotic remodeling [66,67,154–159].

Conclusions and outlook—In summary, we find that simple physical interactions at the interfaces of membrane-enclosed cellular compartments lead to the selective transmission of information, permitting the binary classification of surface regions. In particular, we report that short-range repulsion between membrane-embedded particles, such as arising from shielded electrostatic repulsion [160] or membrane-mediated interactions [51,161,162], produces a sigmoidal mapping between nonuniform external energies and the particle densities that form in response. We show how the nonlinear amplification of environmental heterogeneities is controlled by the effective interaction range of the particles and their total number relative to the surface size, and we identify a regime of optimal information transmission for this physical thresholding, as determined by the gain and threshold of the sigmoid. Indeed, many surface-associated subcellular structures fall within the optimal regime based on their sizes and typical cellular concentrations, and our own measurements of *S. arctica* nuclear pore complex distributions reveal sigmoidal density profiles associated with extranuclear microtubule filaments. Interestingly, membrane-associated proteins often interact with irregularly shaped structures such as filamentous networks leading to quasi-1D interactions that facilitate the capacity for physical thresholding [163,164]. How coupling between structures of different effective dimensions influences biological processes and functions has also been investigated in the context of chemical reaction networks [165,166] and macromolecular assembly [167].

Thresholding filters are used in control circuits, bandpass filters, and neural networks, e.g., to introduce nonlinearities, and compress outputs [168,169]. It will be interesting to investigate how sigmoidal particle distributions interact with downstream cellular processes, aiding pattern recognitionlike functions of compartment surfaces. The selective transmission of information at the cell surface could guide, for example, directed movements in response to external gradients in mechanical or chemical properties.

Analyzing other types of particle interactions could reveal whether more complex transformations are possible that would permit operations such as edge detection or object recognition. We anticipate that our increasing technical ability to measure molecular patterns in cells at the sub-μm scale will enable the discovery of new physical information processing modalities through which cells and subcellular structures perceive their complex surroundings.

Acknowledgments—We thank Tim Dullweber, Ian Estabrook, Isabella Graf, Pamela Guruciaga, Patrick Jentsch, Johannes Jung, Thomas Quail, Jan Rombouts, Sacha Sokoloski, and Laeschkir Würthner for useful discussions and feedback on the manuscript, and Omaya Dudin for his advice and expertise. All authors acknowledge funding from the EMBL. H. S. was supported by the EMBL Interdisciplinary Postdoctoral Fellowship (EIPOD4) programme under Marie Sklodowska-Curie Actions Cofund (Grant Agreement No. 847543). G. D. and H. S. are supported by the European Union (ERC, KaryodynEvo, No. 101078291).

Data availability—The data that support the findings of this article are openly available [146].

[1] K. P. Adamala, M. Dogterom, Y. Elani, P. Schwille, M. Takinoue, and T.-Y. D. Tang, Nat. Rev. Mol. Cell Biol. **25**, 162 (2024).
[2] C. E. Shannon, Bull. Am. Math. Soc. **64**, 123 (1958).
[3] K. D. Farnsworth, J. Nelson, and C. Gershenson, Acta Biotheoretica **61**, 203 (2013).
[4] I. R. Graf and B. B. Machta, Proc. Natl. Acad. Sci. U.S.A. **121**, e2308215121 (2024).
[5] T. Dullweber and A. Erzberger, Curr. Opin. Syst. Biol. **32–33**, 100445 (2023).
[6] S. Uda, Biophys. Rev. Lett. **12**, 377 (2020).
[7] J. Estrada, F. Wong, A. DePace, and J. Gunawardena, Cell **166**, 234 (2016).
[8] C. Collinet and T. Lecuit, Nat. Rev. Mol. Cell Biol. **22**, 245 (2021).
[9] A. Ganesan and J. Zhang, Protein Sci. **21**, 918 (2012).
[10] R. Cheong, A. Rhee, C. J. Wang, I. Nemenman, and A. Levchenko, Science **334**, 354 (2011).
[11] M. D. Brennan, R. Cheong, and A. Levchenko, Science **338**, 334 (2012).
[12] M. Kramar, L. Hahn, A. M. Walczak, T. Mora, and M. Coppey, arXiv:2410.22571.
[13] A. Nandan, A. Das, R. Lott, and A. Koseska, eLife **11**, e76825 (2022).
[14] G. Tkačik and P. R. t. Wolde, Annu. Rev. Biophys. **54**, 249 (2025).
[15] G. Falasco, R. Rao, and M. Esposito, Phys. Rev. Lett. **121**, 108301 (2018).
[16] F. Avanzini, T. Aslyamov, E. Fodor, and M. Esposito, J. Chem. Phys. **161**, 174108 (2024).
[17] D. B. Brückner and G. Tkačik, Proc. Natl. Acad. Sci. U.S.A. **121**, e2322326121 (2024).
[18] L. Wolpert, Dev. Genet. **15**, 485 (1994).
[19] J. O. Dubuis, G. Tkačik, E. F. Wieschaus, T. Gregor, and W. Bialek, Proc. Natl. Acad. Sci. U.S.A. **110**, 16301 (2013).
[20] G. Tkačik and T. Gregor, Development **148**, dev176065 (2021).
[21] L. McGough, H. Casademunt, M. Nikolić, Z. Aridor, M. D. Petkova, T. Gregor, and W. Bialek, PRX Life **2**, 013016 (2024).
[22] G. P. Flowers and C. M. Crews, Dev. Dyn. **249**, 465 (2020).
[23] K. Zieske and P. Schwille, eLife **3**, e03949 (2014).
[24] M. C. Wigbers, T. H. Tan, F. Brauns, J. Liu, S. Z. Swartz, E. Frey, and N. Fakhri, Nat. Phys. **17**, 578 (2021).
[25] L. Wettmann and K. Kruse, Phil. Trans. R. Soc. B **373**, 20170111 (2018).
[26] A. Haupt and N. Minc, J. Cell Sci. **131**, jcs214015 (2018).
[27] P. Rangamani, A. Lipshtat, E. U. Azeloglu, R. C. Calizo, M. Hu, S. Ghassemi, J. Hone, S. Scarlata, S. R. Neves, and R. Iyengar, Cell **154**, 1356 (2013).
[28] C. G. Evans, J. O'Brien, E. Winfree, and A. Murugan, Nature (London) **625**, 500 (2024).
[29] T. Mijatović, A. R. Kok, J. W. Zwanikken, and M. Bauer, arXiv:2505.07641.
[30] R. Braz Teixeira, G. Carugno, I. Neri, and P. Sartori, Proc. Natl. Acad. Sci. U.S.A. **121**, e2320504121 (2024).
[31] D. S. Banerjee, M. J. Falk, M. L. Gardel, A. M. Walczak, T. Mora, and S. Vaikuntanathan, arXiv:2504.15107.
[32] J. Rombouts, J. Elliott, and A. Erzberger, EMBO Rep. **24**, e57739 (2023).
[33] E. Sitarska, S. D. Almeida, M. S. Beckwith, J. Stopp, J. Czuchnowski, M. Siggel, R. Roessner, A. Tschanz, C. Ejsing, Y. Schwab, J. Kosinski, M. Sixt, A. Kreshuk, A. Erzberger, and A. Diz-Muñoz, Nat. Commun. **14**, 5644 (2023).
[34] E. R. Gomes, S. Jani, and G. G. Gundersen, Cell **121**, 451 (2005).
[35] E. Vercruysse, D. B. Brückner, M. Gómez-González, A. Remson, M. Luciano, Y. Kalukula, L. Rossetti, X. Trepat, E. Hannezo, and S. Gabriele, Nat. Phys. **20**, 1492 (2024).
[36] J. d'Alessandro, A. Barbier-Chebbah, V. Cellerin, O. Benichou, R. M. Mège, R. Voituriez, and B. Ladoux, Nat. Commun. **12**, 4118 (2021).
[37] J. E. Ron, M. Crestani, J. M. Kux, J. Liu, N. Al-Dam, P. Monzo, N. C. Gauthier, P. J. Sáez, and N. S. Gov, Nat. Phys. **20**, 501 (2024).
[38] Y. Han, X. Liu, S. Qu, X. Duan, Y. Xiang, N. Jiang, S. Yang, X. Fang, L. Xu, H. Wen, Y. Yu, S. Huang, J. Huang, and K. Zhu, Cell **188**, 3459 (2025).
[39] M. V. Baranov, M. Kumar, S. Sacanna, S. Thutupalli, and G. van den Bogaart, Front. Immunol. **11**, 607945 (2021).
[40] J. L. Stow and N. D. Condon, Clin. Transl. Immunol. **5**, e71 (2016).
[41] S. Cho, J. Irianto, and D. E. Discher, J. Cell Biol. **216**, 305 (2017).
[42] T. Burkart, M. C. Wigbers, L. Würthner, and E. Frey, Nat. Rev. Phys. **4**, 511 (2022).
[43] A. Shellard and R. Mayor, Trends Cell Biol. **30**, 852 (2020).
[44] A. G. Clark, A. Maitra, C. Jacques, M. Bergert, C. Pérez-González, A. Simon, L. Lederer, A. Diz-Muñoz, X. Trepat, R. Voituriez, and D. M. Vignjevic, Nat. Mater. **21**, 1200 (2022).
[45] S. B. Carter, Nature (London) **213**, 256 (1967).
[46] X. Luo, V. Seveau de Noray, L. Aoun, M. Biarnes-Pelicot, P.-O. Strale, V. Studer, M.-P. Valignat, and O. Theodoly, J. Cell Sci. **133**, jcs242883 (2020).
[47] I. C. Fortunato, D. B. Brückner, S. Grosser, L. Rossetti, M. Bosch-Padrós, J. Trebicka, P. Roca-Cusachs, R. Sunyer,

E. Hannezo, and X. Trepat, bioRxiv 10.1101/2024.12.02.626413 (2024).
[48] R. J. Leiphart, D. Chen, A. P. Peredo, A. E. Loneker, and P. A. Janmey, Langmuir **35**, 7509 (2019).
[49] C. Ji and Y. Huang, Commun. Biol. **6**, 1169 (2023).
[50] W.-J. Rappel and L. Edelstein-Keshet, Curr. Opin. Syst. Biol. **3**, 43 (2017).
[51] C. Yolcu, R. C. Haussman, and M. Deserno, Adv. Colloid Interface Sci. **208**, 89 (2014).
[52] M. A. S. Karal, M. M. Billah, M. Ahmed, and M. K. Ahamed, Soft Matter **19**, 8285 (2023).
[53] R. L. Liboff, Phys. Fluids **2**, 40 (1959).
[54] J. Rowlinson, Physica (Amsterdam) **156A**, 15 (1989).
[55] R. Milo and R. Phillips, *Cell Biology by the Numbers* (Garland Science, New York, 2015), Chap. 1.
[56] V. P. Zhdanov, Mol. Biosyst. **5**, 638 (2009).
[57] M. Hu, J. J. Briguglio, and M. Deserno, Biophys. J. **102**, 1403 (2012).
[58] H. Wennerström, E. Vallina Estrada, J. Danielsson, and M. Oliveberg, Proc. Natl. Acad. Sci. U.S.A. **117**, 10113 (2020).
[59] See Supplemental Material at http://link.aps.org/supplemental/10.1103/ywr6-mzz5 for further details, which include also Refs. [60–64].
[60] J. Elliott, Elliott2025 *Mathematica* files, https://git.embl.de/elliot/Elliott2025-Mathematica-Files (2025).
[61] *Mathematica*, Version 14.0, W. R. Inc., Champaign, IL, 2024.
[62] M. Olivetta and O. Dudin, Curr. Biol. **33**, 1597 (2023).
[63] A. Ondracka, O. Dudin, and I. Ruiz-Trillo, Curr. Biol. **28**, 1964 (2018).
[64] D. Gambarotto, F. U. Zwettler, M. Le Guennec, M. Schmidt-Cernohorska, D. Fortun, S. Borgers, J. Heine, J.-G. Schloetel, M. Reuss, M. Unser, E. S. Boyden, M. Sauer, V. Hamel, and P. Guichard, Nat. Methods **16**, 71 (2018).
[65] R. Seelaboyina and R. Vishwakarma, in *ICDSMLA 2021*, edited by A. Kumar, S. Senatore, and V. K. Gunjan (Springer Nature, Singapore, 2023), pp. 23–29.
[66] O. Dudin, A. Ondracka, X. Grau-Bové, A. A. Haraldsen, A. Toyoda, H. Suga, J. Bråte, and I. Ruiz-Trillo, eLife **8**, e49801 (2019).
[67] H. Shah, M. Olivetta, C. Bhickta, P. Ronchi, M. Trupinić, E. C. Tromer, I. M. Tolić, Y. Schwab, O. Dudin, and G. Dey, Nature (London) **630**, 116 (2024).
[68] J. Halatek and E. Frey, Nat. Phys. **14**, 507 (2018).
[69] F. Brauns, J. Halatek, and E. Frey, Phys. Rev. X **10**, 041036 (2020).
[70] C. W. Gardiner, *Stochastic Methods: A Handbook for the Natural and Social Sciences* (Springer, Berlin, 2010), Chap. 13.
[71] R. Belousov, A. Hassanali, and É. Roldán, Phys. Rev. E **106**, 014103 (2022).
[72] A. H. Carter, *Classical and Statistical Thermodynamics* (Pearson Education, Philadelphia, 2000).
[73] L. D. Landau and E. M. Lifshitz, *Statistical Physics*, 3rd ed. (Butterworth-Heinemann, Oxford, 1996), p. 134.
[74] T. L. Hill, *An Introduction to Statistical Thermodynamics* (Dover Publications, Mineola, NY, 1987), p. 128.
[75] N. Tishby, F. C. Pereira, and W. Bialek, arXiv:physics/0004057.
[76] M. Bauer and W. Bialek, PRX Life **1**, 023005 (2023).
[77] M. Bauer, Biochem. Soc. Trans. **50**, 1365 (2022).
[78] M. Kleinman, T. Wang, D. Xiao, E. Feghhi, K. Lee, N. Carr, Y. Li, N. Hadidi, C. Chandrasekaran, and J. C. Kao, bioRxiv, 10.1101/2023.07.12.548742 (2025).
[79] R. Mancini, in *Op Amps for Everyone (Second Edition)*, edited by R. Mancini, 2nd ed. (Newnes, Burlington, 2003), pp. 67–75.
[80] H. Touchette, Phys. Rep. **478**, 1 (2009).
[81] J. Elliott, Elliott2025 metropolis simulations, https://git.embl.de/elliot/Elliott2025-Metropolis-Simulations (2025).
[82] S. Lembo, L. Strauss, D. Cheng, J. Vermeil, M. Siggel, M. Toro-Nahuelpan, C. J. Chan, J. Kosinski, M. Piel, O. Du Roure, J. Heuvingh, J. Mahamid, and A. Diz-Muñoz, bioRxiv, 10.1101/2023.01.31.526409 (2023).
[83] P. Robert, M. Biarnes-Pelicot, N. Garcia-Seyda, P. Hatoum, D. Touchard, S. Brustlein, P. Nicolas, B. Malissen, M.-P. Valignat, and O. Theodoly, Front. Bioeng. Biotechnol. **9**, 625366 (2021).
[84] B. L. Ekerdt, R. A. Segalman, and D. V. Schaffer, Biotechnol. J. **8**, 1411 (2013).
[85] B.-A. Truong Quang, M. Mani, O. Markova, T. Lecuit, and P.-F. Lenne, Curr. Biol. **23**, 2197 (2013).
[86] C. A. Janeway, Jr., P. Travers, M. Walport *et al.*, in *Immunobiology: The Immune System in Health and Disease*, 5th ed. (Garland Science, New York, 2001), Chap. Antigen recognition by T cells.
[87] X. Jiang, S. Dudzinski, K. E. Beckermann, K. Young, E. McKinley, J. O. McIntyre, J. C. Rathmell, J. Xu, and J. C. Gore, J. ImmunoTher. Cancer **8**, e000328 (2020).
[88] M. Swamy, E. P. Dopfer, E. Molnar, B. Alarcón, and W. W. A. Schamel, Scand. J. Immunol. **67**, 418 (2008).
[89] V. P.-Y. Ma, Y. Hu, A. V. Kellner, J. M. Brockman, A. Velusamy, A. T. Blanchard, B. D. Evavold, R. Alon, and K. Salaita, Sci. Adv. **8**, eabg4485 (2022).
[90] T. M. Bui, H. L. Wiesolek, and R. Sumagin, J. Leukoc. Biol. **108**, 787 (2020).
[91] G. Kurz-Isler, T. Voigt, and H. Wolburg, Cell Tissue Res. **268**, 267 (1992).
[92] D. A. Goodenough and J. P. Revel, J. Cell Biol. **45**, 272 (1970).
[93] A. Kuntze, O. Goetsch, B. Fels, K. Najder, A. Unger, M. Wilhelmi, S. Sargin, S. Schimmelpfennig, I. Neumann, A. Schwab, and Z. Pethő, Front. Physiol. **11**, 89 (2020).
[94] E. M. Mulhall, A. Gharpure, R. M. Lee, A. E. Dubin, J. S. Aaron, K. L. Marshall, K. R. Spencer, M. A. Reiche, S. C. Henderson, T.-L. Chew, and A. Patapoutian, Nature (London) **620**, 1117 (2023).
[95] V. Rizzo, C. Morton, N. DePaola, J. E. Schnitzer, and P. F. Davies, Am. J. Physiol. Heart Circ. Physiol. **285**, H1720 (2003).
[96] P. Thomsen, K. Roepstorff, M. Stahlhut, and B. van Deurs, Mol. Biol. Cell **13**, 238 (2002).
[97] C. A. Mannella, Int. J. Mol. Sci. **22**, 1685 (2021).
[98] S. Hiller, J. Abramson, C. Mannella, G. Wagner, and K. Zeth, Trends Biochem. Sci. **35**, 514 (2010).
[99] M. R. Wozny, A. Di Luca, D. R. Morado, A. Picco, R. Khaddaj, P. Campomanes, L. Ivanović, P. C. Hoffmann, E. A. Miller, S. Vanni, and W. Kukulski, Nature (London) **618**, 188 (2023).

[100] Y. Lyu, S. Chen, Y. Zhao, H. Yuan, C. Zhang, C. Zhang, and Q. Meng, Phys. Chem. Chem. Phys. **26**, 12552 (2024).
[101] E. H. Mojumdar, C. Grey, and E. Sparr, Int. J. Mol. Sci. **21**, 56 (2020).
[102] S. Evans, D. Goldman, S. Heinemann, and J. Patrick, J. Biol. Chem. **262**, 4911 (1987).
[103] D. K. McMahon, P. A. Anderson, R. Nassar, J. B. Bunting, Z. Saba, A. E. Oakeley, and N. N. Malouf, Am. J. Physiol. Cell Physiol. **266**, C1795 (1994).
[104] M. M. S. Lo, E. A. Barnard, and J. O. Dolly, Biochemistry **21**, 2210 (1982).
[105] L. Geng, H. L. Zhang, and H. B. Peng, BMC Neurosci. **10**, 80 (2009).
[106] C. Kerntke, F. Nimmerjahn, and M. Biburger, Front. Immunol. **11**, 118 (2020).
[107] V. Wacleche, C. Tremblay, J.-P. Routy, and P. Ancuta, Viruses **10**, 65 (2018).
[108] F. Saji, Rev. Reprod. **4**, 81 (1999).
[109] F. Zhang, S. Wang, L. Yin, Y. Yang, Y. Guan, W. Wang, H. Xu, and N. Tao, Anal. Chem. **87**, 9960 (2015).
[110] A. Abulrob, Z. Lu, E. Baumann, D. Vobornik, R. Taylor, D. Stanimirovic, and L. J. Johnston, J. Biol. Chem. **285**, 3145 (2010).
[111] U. Horzum, B. Ozdil, and D. Pesen-Okvur, MethodsX **1**, 56 (2014).
[112] T. N. TruongVo, R. M. Kennedy, H. Chen, A. Chen, A. Berndt, M. Agarwal, L. Zhu, H. Nakshatri, J. Wallace, S. Na, H. Yokota, and J. E. Ryu, J. Micromech. Microeng. **27**, 035017 (2017).
[113] H. P. Erickson, Biol. Proced. Online **11**, 32 (2009).
[114] T. M. Cover and J. A. Thomas, *Elements of Information Theory*, 99th ed., Wiley Series in Telecommunications and Signal Processing (John Wiley & Sons, Nashville, 1991).
[115] T. Hohmann and F. Dehghani, Cells **8**, 362 (2019).
[116] Y. Cho, D. Haraguchi, K. Shigetomi, K. Matsuzawa, S. Uchida, and J. Ikenouchi, J. Cell Biol. **221**, e202009037 (2022).
[117] M. Resnik-Docampo, C. L. Koehler, R. I. Clark, J. M. Schinaman, V. Sauer, D. M. Wong, S. Lewis, C. D'Alterio, D. W. Walker, and D. L. Jones, Nat. Cell Biol. **19**, 52 (2017).
[118] J. Howard, Annu. Rev. Biophys. **38**, 217 (2009).
[119] X. Sun and G. M. Alushin, FEBS J. **290**, 2576 (2023).
[120] F. Bosveld, O. Markova, B. Guirao, C. Martin, Z. Wang, A. Pierre, M. Balakireva, I. Gaugue, A. Ainslie, N. Christophorou, D. K. Lubensky, N. Minc, and Y. Bellaïche, Nature (London) **530**, 495 (2016).
[121] R. X. Norman, Y.-C. Chen, E. E. Recchia, J. Loi, Q. Rosemarie, S. L. Lesko, S. Patel, N. Sherer, M. Takaku, M. E. Burkard, and A. Suzuki, J. Cell Biol. **224**, e202407116 (2025).
[122] N. Radmacher, A. I. Chizhik, O. Nevskyi, J. I. Gallea, I. Gregor, and J. Enderlein, Annu. Rev. Biophys. **54**, 163 (2025).
[123] Z. Dai, X. Luo, H. Xie, and H. B. Peng, J. Cell Biol. **150**, 1321 (2000).
[124] Y. Chen, F. C. Ip, L. Shi, Z. Zhang, H. Tang, Y. P. Ng, W.-C. Ye, A. K. Fu, and N. Y. Ip, J. Neurosci. **34**, 2413 (2014).
[125] G. Xing, H. Jing, L. Zhang, Y. Cao, L. Li, K. Zhao, Z. Dong, W. Chen, H. Wang, R. Cao, W.-C. Xiong, and L. Mei, eLife **8**, e49180 (2019).
[126] R. B. Troyanovsky, I. Indra, and S. M. Troyanovsky, Nat. Commun. **16**, 1801 (2025).
[127] M. L. Dustin and J. A. Cooper, Nat. Rev. Immunol. **1**, 23 (2000).
[128] L. Celli, J.-J. Ryckewaert, E. Delachanal, and A. Duperray, J. Immunol. **177**, 4113 (2006).
[129] O. Carpén, P. Pallai, D. E. Staunton, and T. A. Springer, J. Cell Biol. **118**, 1223 (1992).
[130] E. Y. Kirichenko, S. N. Skatchkov, and A. M. Ermakov, Biochem. (Moscow), Suppl. Ser. A: Membrane Cell Biol. **15**, 107 (2021).
[131] B. Alberts, D. Bray, J. Lewis, M. Raff, K. Roberts, and J. Watson, *Molecular Biology of the Cell*, 4th ed. (Garland, New York, 2002), Chap. Cell Junctions.
[132] J. Y. Cheema, J. He, W. Wei, and C. Fu, Contact **4**, 25152564211064491 (2021).
[133] E. Dultz, M. Wojtynek, O. Medalia, and E. Onischenko, Cells **11**, 1456 (2022).
[134] S. Bahmanyar and C. Schlieker, Mol. Biol. Cell **31**, 1315 (2020).
[135] A. K. Balaji, S. Saha, S. Deshpande, D. Poola, and K. Sengupta, Front. Cell Dev. Biol. **10**, 1068347 (2022).
[136] M. Soheilypour, M. Peyro, Z. Jahed, and M. R. K. Mofrad, Cell. Mol. Bioeng. **9**, 217 (2016).
[137] S. Biedzinski, G. Agsu, B. Vianay, M. Delord, L. Blanchoin, J. Larghero, L. Faivre, M. Théry, and S. Brunet, EMBO J. **39**, e103957 (2020).
[138] J. Geng, Z. Kang, Q. Sun, M. Zhang, P. Wang, Y. Li, J. Li, B. Su, and Q. Wei, Research **6**, 0054 (2023).
[139] Y. Maizels and G. Gerlitz, FEBS J. **282**, 3500 (2015).
[140] A. Nair, J. Khanna, J. Kler, R. Ragesh, and K. Sengupta, Nucleus **16**, 2449520 (2025).
[141] M. W. Goldberg, Semin. Cell Dev. Biol. **68**, 52 (2017).
[142] P. Huang, X. Zhang, Z. Cheng, X. Wang, Y. Miao, G. Huang, Y.-F. Fu, and X. Feng, Plant Cell **36**, 346 (2024).
[143] Y. Guo and Y. Zheng, Mol. Biol. Cell **26**, 3379 (2015).
[144] L. M. Hoffman, M. A. Smith, C. C. Jensen, M. Yoshigi, E. Blankman, K. S. Ullman, and M. C. Beckerle, Mol. Biol. Cell **31**, 1774 (2020).
[145] F. Donnaloja, E. Jacchetti, M. Soncini, and M. T. Raimondi, Front. Physiol. **10**, 896 (2019).
[146] J. Elliott, H. Shah, R. Belousov, G. Dey, and A. Erzberger, Image dataset used in 'Repulsive particle interactions enable selective information processing at cellular interfaces,' https://www.ebi.ac.uk/biostudies/bioimages/studies/S-BIAD2081 (2025).
[147] J. Elliott, Elliott2025 image analysis s-arctica, https://git.embl.de/elliot/Elliott2025-Image-Analysis-S-arctica (2025).
[148] L. Li, J. Alper, and E. Alexov, Sci. Rep. **6**, 31523 (2016).
[149] J. Schindelin, I. Arganda-Carreras, E. Frise, V. Kaynig, M. Longair, T. Pietzsch, S. Preibisch, C. Rueden, S. Saalfeld, B. Schmid, J.-Y. Tinevez, D. J. White, V. Hartenstein, K. Eliceiri, P. Tomancak, and A. Cardona, Nat. Methods **9**, 676 (2012).

[150] N. Daigle, J. Beaudouin, L. Hartnell, G. Imreh, E. Hallberg, J. Lippincott-Schwartz, and J. Ellenberg, J. Cell Biol. **154**, 71 (2001).
[151] G. Rabut, V. Doye, and J. Ellenberg, Nat. Cell Biol. **6**, 1114 (2004).
[152] B. H. Toyama and M. W. Hetzer, Nat. Rev. Mol. Cell Biol. **14**, 55 (2013).
[153] J. M. Varberg, J. R. Unruh, A. J. Bestul, A. A. Khan, and S. L. Jaspersen, Life Sci. Alliance **5**, e202201423 (2022).
[154] D. M. Roth, G. W. Moseley, D. Glover, C. W. Pouton, and D. A. Jans, Traffic **8**, 673 (2007).
[155] D. M. Roth, G. W. Moseley, C. W. Pouton, and D. A. Jans, J. Biol. Chem. **286**, 14335 (2011).
[156] M. E. Kelley, L. Carlini, N. Kornakov, A. Aher, A. Khodjakov, and T. M. Kapoor, Mol. Biol. Cell **35**, ar48 (2024).
[157] G. Gerlitz, O. Reiner, and M. Bustin, Cell Mol. Life Sci. **70**, 1255 (2013).
[158] D. Velasquez-Carvajal, F. Garampon, L. Besnardeau, R. Lemée, S. Schaub, and S. Castagnetti, J. Cell Sci. **137**, jcs261733 (2024).
[159] H. Maiato, P. Sampaio, and C. E. Sunkel Int. Rev. Cytol. **241**, 53 (2004).
[160] L. Johannes, W. Pezeshkian, J. H. Ipsen, and J. C. Shillcock, Trends Cell Biol. **28**, 405 (2018).
[161] A. Shrestha, O. Kahraman, and C. A. Haselwandter, Phys. Rev. E **105**, 054410 (2022).
[162] J. M. Barakat and T. M. Squires, Langmuir **38**, 1099 (2022).
[163] D. Pérez-Sala and M. Guo, Front. Cell Dev. Biol. **10**, 1103110 (2022).
[164] B. Alberts, A. Johnson, J. Lewis, M. Raff, K. Roberts, and P. Walter, *Molecular Biology of the Cell*, 4th ed. (Garland Science, New York, 2002), Chap. The Self-Assembly and DynamicStructure of Cytoskeletal Filaments.
[165] F. Brauns, G. Pawlik, J. Halatek, J. Kerssemakers, E. Frey, and C. Dekker, Nat. Commun. **12**, 3312 (2021).
[166] L. Würthner, F. Brauns, G. Pawlik, J. Halatek, J. Kerssemakers, C. Dekker, and E. Frey, Proc. Natl. Acad. Sci. U.S.A. **119**, e2206888119 (2022).
[167] N. Banterle, A. P. Nievergelt, S. de Buhr, G. N. Hatzopoulos, C. Brillard, S. Andany, T. Hübscher, F. A. Sorgenfrei, U. S. Schwarz, F. Gräter, G. E. Fantner, and P. Gönczy, Nat. Commun. **12**, 6180 (2021).
[168] S. R. Dubey, S. K. Singh, and B. B. Chaudhuri, Neurocomputing **503**, 92 (2022).
[169] K. J. Astrom and R. M. Murray, *Feedback Systems* (Princeton University Press, Princeton, NJ, 2008).